# Photoelectron Imaging and Theoretical Study on Nascent Hydrogen Bond Network in Microsolvated Clusters of Au−(CH3OH)(n) (n=1−5)

**ARTICLE** *in* THE JOURNAL OF PHYSICAL CHEMISTRY A · APRIL 2014

Impact Factor: 2.69 · DOI: 10.1021/jp411411j · Source: PubMed

THE JOURNAL OF PHYSICAL CHEMISTRY A

Article

pubs.acs.org/JPCA

# Photoelectron Imaging and Theoretical Study on Nascent Hydrogen Bond Network in Microsolvated Clusters of $Au^-(CH_3OH)_n$ ($n$ = 1−5)

Zhengbo Qin, Ran Cong, Hua Xie, Zhiling Liu, Xia Wu, Zichao Tang,* Ling Jiang,* and Hongjun Fan*

State Key Laboratory of Molecular Reaction Dynamics, Dalian Institute of Chemical Physics, Chinese Academy of Sciences, Dalian 116023, China

Supporting Information

**ABSTRACT:** We first demonstrate the photoelectron spectroscopic evidence of the transition of two competitive solvation patterns in the $Au^-(CH_3OH)_n$ ($n$ = 1−5) clusters. Quantum chemical calculations have been carried out to characterize the geometric structures, energy properties and hydrogen-bonded patterns, and to aid the spectral assignment. It has been found that the nonconventional hydrogen bonds dominate the small clusters ($n$ = 1 and 2), whereas the conventional hydrogen bonds play more and more important role from $n$ = 2 to $n$ = 5. This finding provides concrete hydrogen bond network evolution of $Au^-$ surrounded by methanol molecules.

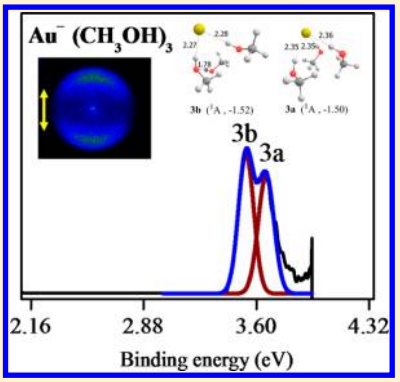


## 1. INTRODUCTION

The investigation of the electronic and geometrical properties of solvated clusters provides molecular level information about the interactions between solvent and solute, which gives insight into the nature of macroscopic properties.[1−5] These solvent molecules have been demonstrated to be able to promote the reactions catalyzed by transition metals. For instance, experimental and theoretical evidence have shown that the presence of solvent molecules on either free or supported gold clusters enhances the catalytic activity for the $O_2$ dissociation, resulting in facilitating the CO oxidation.[6−16]

In the gas-phase experiments, a number of solvated metal ions have been detected through collision-induced dissociation (CID),[17,18] guided ion-beam mass spectrometry (GIBMS),[19] ion/neutral chemistry,[20] high-pressure mass spectrometry (HPMS),[21,22] electron-capture dissociation (ECD),[18,23,24] infrared photodissociation (IRPD) spectroscopy,[1,2] photoelectron spectroscopy (PES),[25−27] etc. In particular, IRPD and PES have been widely used to characterize the structures of the cluster ions.[28−30] Extensive gas-phase spectroscopic and theoretical investigations have been carried out on the solvation of coinage metal ions, especially for gold.[2,31−44] One of the key issues focuses on whether the coinage metal ions are surface solvated or interior solvated states. Coordination and solvation structures of metal cations (i.e., $Mg^+(H_2O)_{1-4}$,[45] $Mg^+(CH_3OH)_{1-4}$,[45] $Ag^+(H_2O)_{1-4}$,[46,47] $Cu^+(H_2O)_{1-7}$,[46,48] and $M^+(H_2O)_{2-5}$ (M = Li, Na, K, and Cs)[49,50]) have been probed via infrared spectroscopy. IRPD studies revealed that the halide anions ($Cl^-$, $Br^-$, $I^-$) prefer the surface solvated state with methanol molecules.[51] So far, much less work has been done for the solvation behavior of coinage metal anions. Surface solvated feature is found to be dominant in the small $M^-(H_2O)_2$ clusters (M = Cu, Ag, Au).[31,37,39,43] Recently, the methanol-methanol hydrogen bond interactions (also nominated conventional hydrogen bonds, HB)[52,53] have been observed in the $Ag^-(CH_3OH)_2$ cluster, even though the ionic hydrogen bonds (also nominated nonconventional hydrogen bonds, NHB)[54,55] dominates the spectrum.[40] However, the geometry-specific transition from ionic hydrogen bonds to conventional hydrogen bonds for such small cluster size has not been identified in photoelectron spectra experiment yet.

In the previous studies of the ion−molecule reactions of $Au^-$ with $H_2O$, $CH_3OH$, and $CH_3SH$, the solvated $[Au\cdots HR]^-$ and inserted $[HAuR]^-$ products have been experimentally observed for R = $SCH_3$, whereas only solvated $[Au\cdots HR]^-$ products have been found for R = $OCH_3$ and OH.[44] In this work, we present a joint photoelectron imaging and *ab initio* calculation study on the solvation growth patterns for the clusters of $Au^-(CH_3OH)_n$ ($n$ = 1−5).

## 2. EXPERIMENTAL AND THEORETICAL METHODS

The experiments were performed using a laser ablation source and photoelectron velocity-map imaging system. The instrument has been described previously.[56] Briefly, the second harmonic of Nd:YAG laser (532 nm, 10 Hz) was focused on the rotating gold target (99.9%) in the presence of a supersonic beam of helium (99.999%) carrier gas with bubbled methanol. The formed anions of interest were steered to a McLaren−Wiley time-of-flight, mass selected, and interacted with a laser beam for the photodetachment. The resulting photoelectrons were extracted by a velocity map imaging photoelectron

Received: November 20, 2013
Revised: April 26, 2014
Published: April 28, 2014

spectrometer and recorded by a charge-coupled device camera. Each image was accumulated with 10 000−50 000 laser shots at a 10 Hz repetition rate. The final raw image stood for the projection of the photoelectron density in the 3D laboratory frame onto the 2D imaging detector. The original 3D distribution was reconstructed using the basis set expansion (BASEX) inverse Abel transform method, and the photoelectron spectra were acquired by integrating the central slice of the 3D distribution.[57] The photoelectron kinetic energy spectra were calibrated by the known spectrum of $Au^-$. The photoelectron spectra (PES) were plotted against electron binding energy eBE = $h\nu$ − eKE, where $h\nu$ is the photon energy. The typical energy resolution was about 30 meV full width at half-maximum (fwhm) at electron kinetic energy (eKE) of 1 eV.

All calculations were carried out using the Gaussian09 program[58] at the double-hybrid density functional theory (mPW2PLYP)[59] with long-range dispersion corrections. Correlation-consistent polarized double-$\zeta$ basis sets with the small core pseudopotentials (cc-pVDZ-pp)[60] were used for gold atom and cc-pVDZ[61−63] for all other atoms. The structures and electronic properties of the $Au^-(CH_3OH)_n$ ($n$ = 0−5) complexes were calculated. Geometry optimizations without any symmetry constraint were performed, and harmonic frequency analyses were performed to verify optimized minima. All the energies of the optimized structures of $Au^-(CH_3OH)_n$ ($n$ = 0−4) were reevaluated with aug-cc-pVTZ-pp[60] basis sets for gold, and aug-cc-pVTZ[61−63] for all other atoms at the same (mPW2PLYP) level. The validity of this computational method has been demonstrated in Au atom. For $Au^-(CH_3OH)_5$, the energies of the optimized structures were reevaluated with aug-cc-pVDZ-pp basis sets for gold, and aug-cc-pVDZ for all other atoms at the mPW2PLYP level. To verify the credibility of VDEs of $Au^-(CH_3OH)_5$ with this basis set, we also conducted calculations with aug-cc-pVDZ and aug-cc-pVTZ basis sets on $Au^-(CH_3OH)_4$ and listed all results in the Supporting Information (Figure S1 and Table S1) for comparison. The vertical detachment energy (VDE) was defined as the energy difference between the ground state of the anion and the ground state of the neutral at the anion geometry. Each total binding energy ($E_b$) has been calculated as the difference between the energy of the complexes and the sum of the energy of the monomers. The counterpoise method was applied to account for basis set superposition error (BSSE)[64,65] in the calculation of the binding energy or solvation energy of the methanol molecules.

## 3. RESULTS AND DISCUSSION

**3.1. Photoelectron Imaging and Spectra.** The 266 nm photoelectron velocity-map images and corresponding photoelectron spectra (PES) of $Au^-(CH_3OH)_n$ ($n$ = 1−5) are presented in Figure 1. Experimental vertical detachment energies (VDEs) are summarized in Table 1. The bands in the photoelectron spectrum represent the electron binding energies of photodetachment transitions from the ground state of the anionic cluster to the ground or excited states of corresponding neutral cluster. Two bands (X and A) present in the $Au^-(CH_3OH)_{1,2}$ clusters, blue-shifting by about 0.49 and 0.94 eV relative to the $Au^-$.[44] Thus, the X and A bands in each cluster should be due to the ground and excited states of the solvated clusters, respectively. In the larger $Au^-(CH_3OH)_{3-5}$ clusters, only X bands are observed, but the A bands are absent because these binding energies are beyond the 266 nm photon energy. With the increase of cluster size, the X bands vary from 2.82 to 4.18 eV (Table 1 and Figure 1). Interestingly, the band widths in the $n$ = 3−5 clusters (fwhm: ∼0.30 eV) are much larger than those in the $n$ = 1 and 2 clusters (fwhm: ∼0.11 eV).

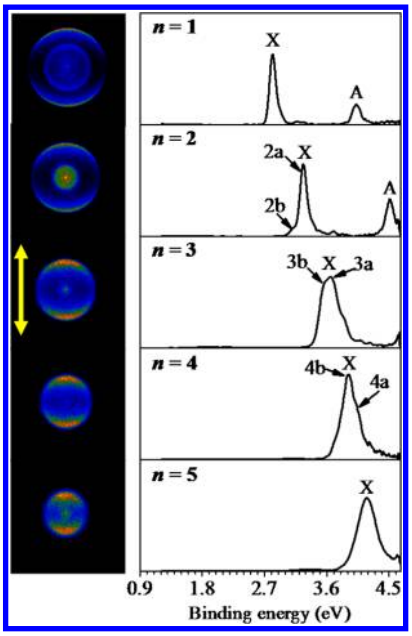


**Figure 1.** Photoelectron images and spectra for $Au^-(CH_3OH)_n$ ($n$ = 1−5) obtained at 266 nm. The left side shows the raw photoelectron image of $Au^-(CH_3OH)_n$. The double arrow shows the direction of the laser polarization.

**Table 1. Theoretical VDEs of the Low-Lying Isomers of $Au^-(CH_3OH)_n$ ($n$ = 0−5) and the Comparison with the Experimental Results**

| | VDE (eV) | | | |
|---|---|---|---|---|
| | expt[a] | | theor[e] | |
| species | 355 nm | 266 nm | aug-cc-pVDZ(pp) | aug-cc-pVTZ(pp) |
| $n$ = 0[b] | 2.31(2) | 2.31(2) | | 2.15 |
| $n$ = 1[b] | 2.80(2) | 2.82(2) | | 2.69 (**1a**) |
| $n$ = 2 | 3.11(2)[c] | 3.11(2) | | 3.05 (**2b**) |
| | 3.25(2)[c] | 3.26(2) | | 3.16 (**2a**) |
| $n$ = 3 | – | | | 3.26 (**3c**) |
| | 3.53(3)[d] | 3.56(3) | | 3.47 (**3b**) |
| | 3.66(3)[d] | 3.67(3) | | 3.61 (**3a**) |
| $n$ = 4 | | | | 3.41 (**4e**) |
| | | | | 3.65 (**4d**) |
| | | | | 3.70 (**4c**) |
| | | 3.91(3) | | 3.88 (**4b**) |
| | | 4.04(3) | | 3.99 (**4a**) |
| $n$ = 5 | | | 3.51 (**5g**) | |
| | | | 3.77 (**5f**) | |
| | | | 3.88 (**5e**) | |
| | | | 4.02 (**5d**) | |
| | | | 4.12 (**5c**) | |
| | | 4.18(3) | 4.22 (**5b**) | |
| | | | 4.32 (**5a**) | |

[a]Numbers in parentheses are experimental uncertainties in the last digit. [b]Reference 44. [c]Reference 66. [d]Detachment laser wavelength is 313.5 nm. [e]Black bold numbers in parentheses stand for different isomers.

Figure 2 shows the 313.5 nm photoelectron velocity-map image and corresponding PES spectrum of the $Au^-(CH_3OH)_3$


dx.doi.org/10.1021/jp411411j | J. Phys. Chem. A 2014, 118, 3402−3409

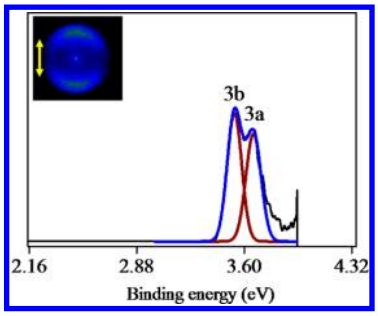


**Figure 2.** Photoelectron image and spectrum for $Au^-(CH_3OH)_3$ obtained at 313.5 nm (3.955 eV). The left side shows the raw photoelectron image of $Au^-(CH_3OH)_3$. The double arrow shows the direction of the laser polarization. Spectral peak fitting is shown for $n = 3$. Black plot denotes experimental data. Brown line denotes the fitting of individual isomer. Blue line denotes the fitting of both isomers.

cluster. Two peaks with similar intensities are observed at 3.53 and 3.66 eV, respectively. In contrast with smaller clusters, only one sharp peak at 2.80 eV has been observed in $Au^-(CH_3OH)$,[44] while one sharp peak at 3.25 eV with one shoulder at 3.11 eV in $Au^-(CH_3OH)_2$,[66] implying the difference in the solvation feature among these clusters.

**3.2. Features of Optimized Structures.** Quantum chemical calculations were carried out to aid the experimental assignments. Considering that the VDEs of **2a** and **2b** calculated at mPW2PLYP/aug-cc-pVTZ(pp) level (3.05 and 3.16 eV) are much closer to the experiments (3.11 and 3.25 eV at 313.5 nm) (Table 1) than those at MP2/aug-cc-pVTZ(pp) level (3.36 and 3.53 eV),[66] the results calculated by the mPW2PLYP/aug-cc-pVTZ(pp) method are used for the present work. Optimized geometric structures and total binding energies ($E_b$) of $Au^-(CH_3OH)_n$ ($n$ = 1−5) are illustrated in Figure 3 and presented in the Supporting Information (Table S2). The first methanol forms a strong NHB with $Au^-$ (isomer **1a**). For $n$ = 2, there are two low-lying solvation structures with slight relative energy difference of 0.02 eV: (1) in structure **2a**, two methanol molecules individually bind with $Au^-$ without solvent−solvent hydrogen interaction (Figure 3), forming two identical NHB, and (2) in structure **2b**, one methanol molecule binds closely with $Au^-$ and forms a solvent−solvent hydrogen bond with the second methanol molecule. For $n$ = 3, the most stable structure (**3b**) consists of a methanol monomer and a methanol dimer separately binding with $Au^-$, respectively. The next energetically higher structure **3c** involves a hydrogen-bonded network with only one methanol molecule closely binding with $Au^-$. The structure **3a** forms three-coordinate NHB, similar to **2a**. For $n$ = 4, the most stable structures of **4c** and **4d**, calculated to be nearly isoenergetic, consist of two methanol dimer and one methanol trimer, respectively. The isoenergetic structures **4b** and **4e** involve one methanol dimer and one methanol tetramer, respectively, locating +0.04 eV above **4c** and **4d**. The highest energy structure **4a** (+0.09 eV) contains four-coordinate NHB without hydrogen-bonded interaction in between the methanol molecules. In the case of $n$ = 5, the most stable structure is **5e** including a methanol dimer and a trimer. The nearly isoenergetic structures of **5c**, **5d**, and **5g** locate about +0.02 eV above **5e**. The next high energy structures of **5b** and **5f** are nearly isoenergetic. The highest energy structure **5a** (+0.15 eV) contains five-coordinate non-conventional hydrogen bonds without conventional hydrogen bonds.

In the structures ***n*a** ($n$ = 1−5), the ionic hydrogen bond distances between Au and hydroxyl hydrogen in $CH_3OH$ (NHB) are predicted to gradually increase from 2.28 to 2.45 Å (Figure 3). In all the other structures, the hydrogen bond distances in-between the methanol molecules fall in the range 1.69−1.79 Å, indicating typical HB.[52,67,68]

**3.3. Discussion.** As listed in Table 1, the mPW2PLYP/aug-cc-pVTZ(pp) VDEs of **3a**, **3b**, and **3c** are 3.61, 3.47, and 3.26 eV, respectively, which yield the gaps of 0.14 and 0.21 eV. Two peaks are experimentally observed at 3.66 and 3.53 eV in the 313.5 nm spectrum (Figure 2), giving a separation of 0.13 eV. This suggests that the combination of **3a** and **3b** is closer to the experimental feature than that of **3b** and **3c**. Previous studies show that the contributions for the bands in the 355 nm spectra for $Au^-(CH_3OH)$ and $Au^-(CH_3OH)_2$ are mainly from a single structure (**1a** and **2a**), respectively.[44,66] In contrast, both structures **3a** and **3b** should be responsible for the broader feature of experimental band in $Au^-(CH_3OH)_3$ (Figure 1). Furthermore, the fitting of both structures **3a** and **3b** well reproduces the experiment (Figure 2), supporting the above analysis. Similarly, the contribution for the PES of $Au^-(CH_3OH)_4$ should be from both **4a** and **4b** (Table 1), which is supported by the fitting as shown in Figure 5 and the comparison of VDE values. Although the gaps for both ***n*a** and ***n*b** is 0.11−0.14 eV and experiment and theory differ by about the same energy at $n$ = 2−4, the experimental uncertainties for both ***n*a** and ***n*b** (0.02 eV for $n$ = 2, 0.03 eV for $n$ = 3, and 0.03 eV for $n$ = 4) are less than 0.05 eV. Therefore, the experimental uncertainties of both ***n*a** and ***n*b** cannot overlap each other, which facilitates the structural determination of ***n*a** and ***n*b**. It is also noted that for both ***n*a** and ***n*b** structures experiment gets closer to theory at higher $n$. The underlying calculated method yields reasonable and substantially better results for even larger clusters, which further provide credible evidence for the spectral assignments. For $n$ = 5, due to a broad peak, there is only one determined VDE value of 4.18 eV. It is noted that the theoretical VDEs of **5b**−**5d** get close to the experimental value. The isomer of **5b** most likely accounts for the photoelectron spectrum but we cannot exclude the contributions of **5c,d**.

Two types of solvation patterns could be classified from the above-mentioned analysis. One series of structures ***n*a** ($n$ = 1−5) (type I) feature that the $Au^-$ are solvated by the individual methanol molecules without HB, which could be called as NHB growth pattern. In the series of structures ***n*b** ($n$ = 2−5) (type II), methanol dimer with hydrogen-bonded network (exist HB) are formed and bind to the $Au^-$, which could be called as HB growth pattern. For $n$ = 2, the ratio of peak intensities of **2a** to **2b** in the 266 nm spectra is about 10:1 (Figure 1), indicating that the solvation pattern of type I is dominated in the $Au^-(CH_3OH)_2$ cluster. Interestingly, peak intensities of **3a** and **3b** become nearly identical, showing a competition between type I and type II solvation patterns in $n$ = 3. Increasing the cluster size to $n$ = 4, peak intensity of **4b** turns to be stronger than that of **4a**, showing a dominated feature of type II solvated pattern. In the case of $Au^-(CH_3OH)_5$, the solvated pattern should be similar to $n$ = 4 system.

Predicted VDEs of two types of solvated structures are compared to the experimental values in Figure 4. The curves for the comparison of each type exhibit the monotonic increase of ADE with the increase of methanol molecule. Both solvated states show a similar stepwise increase of VDE in the range of 0.35−0.50 eV. The experimental band of $n$ = 5 is measured to


dx.doi.org/10.1021/jp411411j | J. Phys. Chem. A 2014, 118, 3402−3409

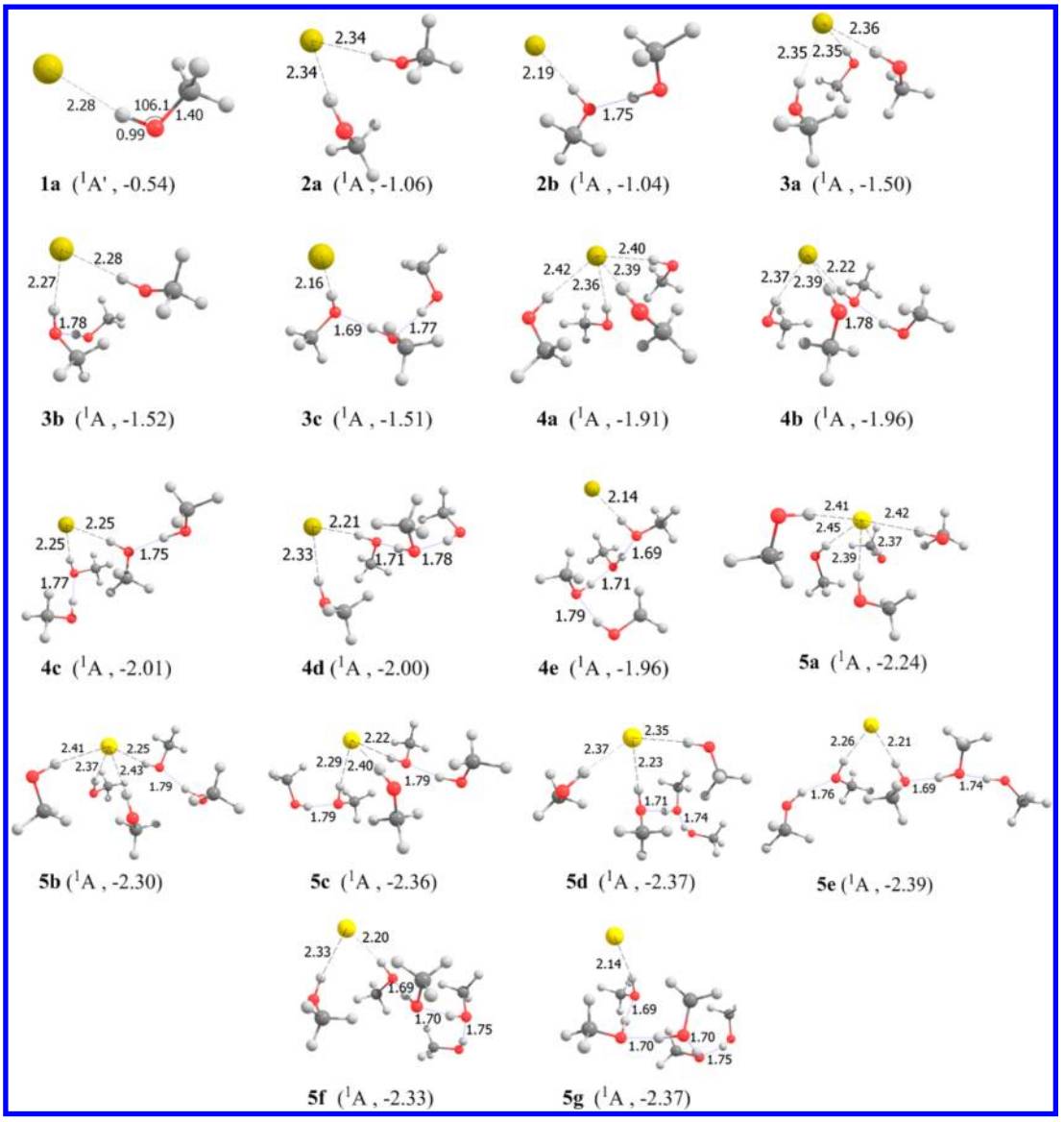


**Figure 3.** Optimized structures (bond lengths in Å and bond angles in degree) at the mPW2PLYP/cc-pVDZ(pp) level and total binding energies ($E_b$, eV) of $Au^-(CH_3OH)_n$ ($n$ = 1–4) at the mPW2PLYP/aug-cc-pVTZ(pp) level and of $Au^-(CH_3OH)_5$ at the mPW2PLYP/aug-cc-pVDZ(pp) level.

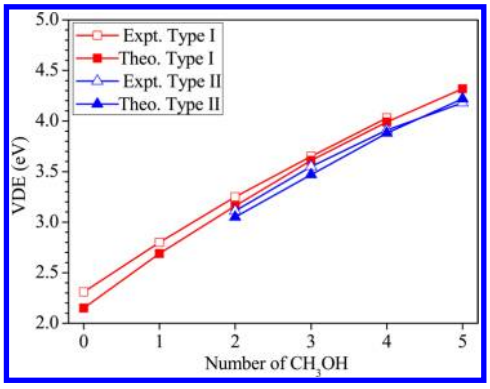


**Figure 4.** Comparison of predicted VDEs of NHB growth pattern (type I) and HB growth pattern (type II) with the experimental values for $Au^-(CH_3OH)_n$ ($n$ = 0–5).

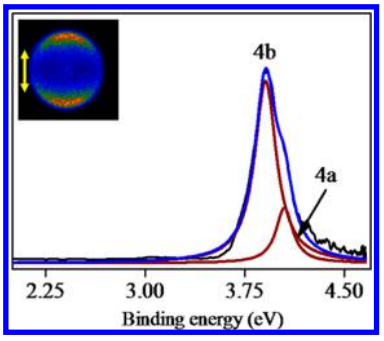


**Figure 5.** Spectral peak fitting for $Au^-(CH_3OH)_4$ (266 nm (4.661 eV)). Black curve stands for the experimental data, wine curve for the fitting of individual isomer, and blue curve for the fitting of both isomers.

be 4.18 eV, which is 0.27 eV higher than the main band centered at 3.91 eV of $n$ = 4. This suggests that the $n$ = 5 clusters should be dominated by the type II solvated pattern. Figure 8 depicts the computed total binding energies ($E_b$) for type I solvated (***n*a**) and type II solvated (***n*b**) patterns. The


dx.doi.org/10.1021/jp411411j | J. Phys. Chem. A 2014, 118, 3402–3409

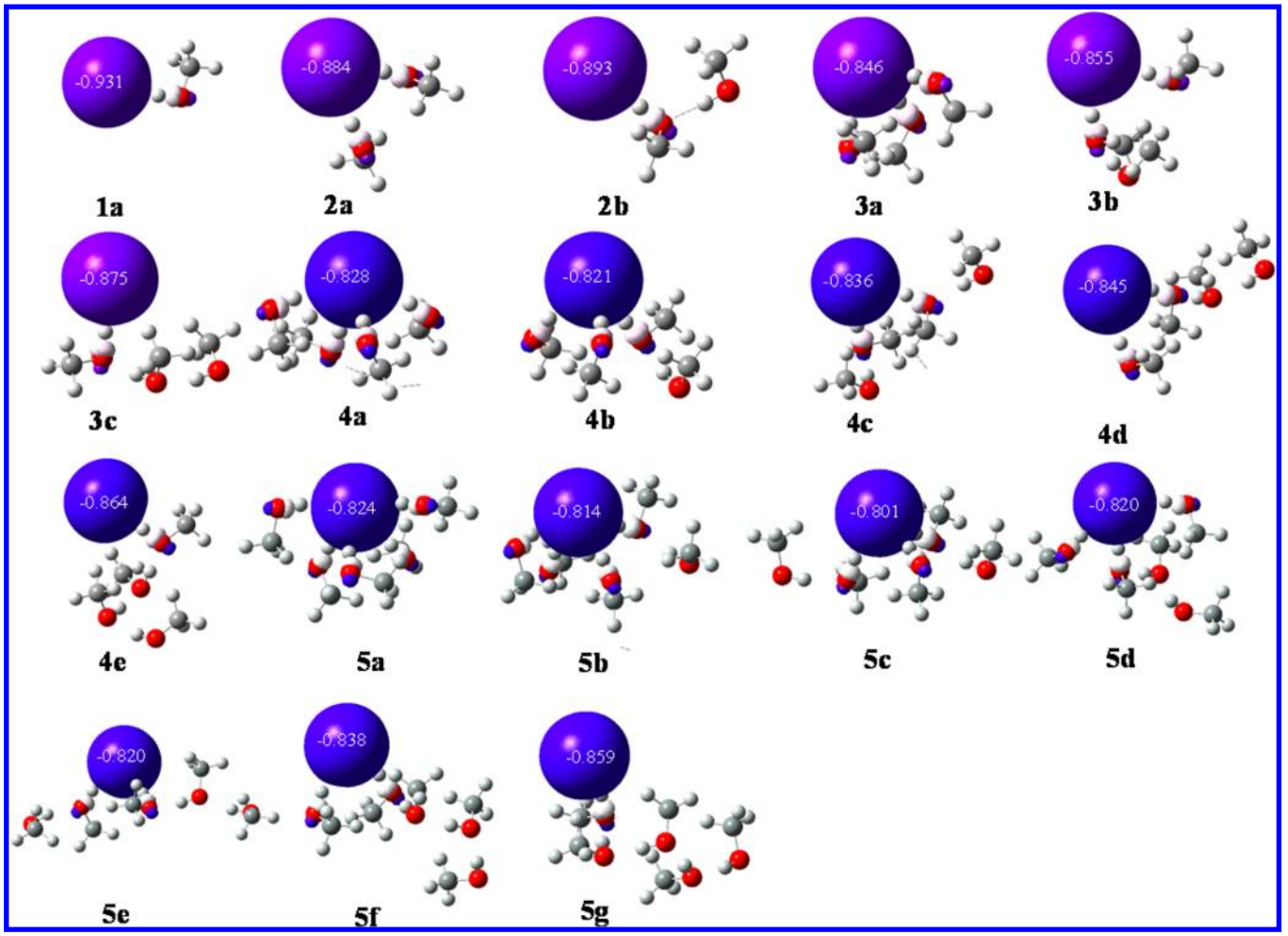


**Figure 6.** HOMOs of $Au^{-}(CH_3OH)_n$ ($n$ = 1−5) (isosurface value = 0.04 au) and natural population analysis (NPA) charge on Au at the mPW2PLYP/cc-pVDZ(pp) level.

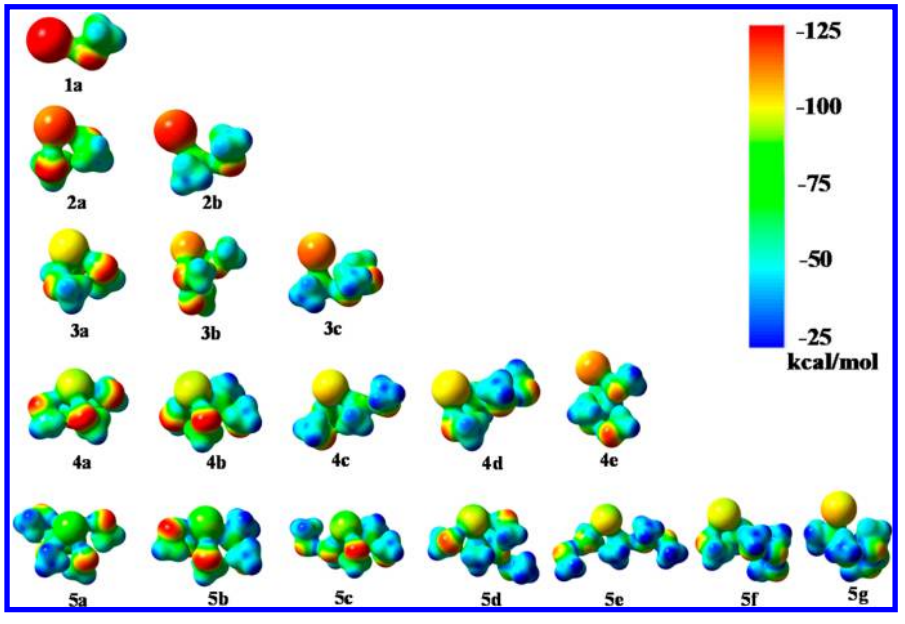


**Figure 7.** Electrostatic potential surface of $Au^{-}(CH_3OH)_n$ ($n$ = 1−5) (density isosurface value = 0.01 au) at the mPW2PLYP/cc-pVDZ(pp) level.

clear tendency shows that the crossover of both curves occurs at $n$ = 3, supporting the above analysis of solvation preference based on the VDEs.

In order to intuitively comprehend the binding character in the experimentally observed isomers of $Au^{-}(CH_3OH)_n$ ($n$ = 1−5), it is illustrative to plot the highest occupied molecular


dx.doi.org/10.1021/jp411411j | J. Phys. Chem. A 2014, 118, 3402−3409

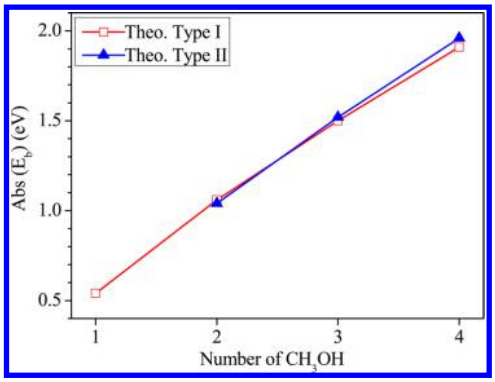


**Figure 8.** Comparison of absolute values of total binding energies ($E_b$, eV) between NHB growth pattern (type I) and HB growth pattern (type II) for $Au^-(CH_3OH)_n$ ($n$ = 1−4).

orbital (HOMO), which accommodates the excess charge (see Figure 6). The interaction between $Au^-$ and $CH_3OH$ in $Au^-(CH_3OH)_n$ ($n$ = 1−5) can be described as metal hydrogen bond in view of HOMO features where Au donates its 6s electrons to the O−H $\sigma^*$ orbital of $CH_3OH$, as shown in Figure 6. As we expected, the number of directly coordinated $CH_3OH$ molecules to $Au^-$ affects the charge transfer capacity from Au anion to $CH_3OH$ molecules. Natural population analysis (NPA)[69] also supports the larger charge transfer in large cluster size than in small cluster size and in ***n*a** system than in ***n*b** system (For $n$ = 4 and 5 cases, it is an exception possibly due to calculated error). As the results, in **5a**, the charge transfer amounts to nearly 0.2 e. Electrostatic potential maps can be used to analyze charge distributions in these clusters. As depicted in Figure 7, although all of these isomers of $Au^-(CH_3OH)_n$ ($n$ = 1−5) (***n*a**−***n*g**) carry identical charges of −1, the electrostatic potential is the most negative around the smallest cluster size anion, $Au^-(CH_3OH)$. As cluster size increases for the same binding motif, such as ***n*a**, the potential becomes steadily less negative, which can account for less negative charge on Au and is consistent with the NPA results. For the same cluster size, the electrostatic potential is less negative from ***n*g** to ***n*a**, which can be the result of the electron donation from the 6s orbital of $Au^-$ to directly coordinated $CH_3OH$ molecules and charge disperse degree on $Au^-$. Thus, experimentally observed type I solvated (***n*a**) and type II solvated (***n*b**) patterns differ by not only geometric structure but also by localizing charge capacity on Au and electrostatic potential.

Even though binding energies of other structures (**3c**, **4c**−**4e**) (Figure 3) are slightly larger than those of **3a** and **4a**, the calculated VDEs of structures **3c** and **4c**−**4e** (Table 1) deviate remarkably from the experimental values, resulting in the absence from the present experimental spectra. In fact, the small energy difference in-between these isomers (0.02 eV for **2a**/**2b**, 0.02 eV for **3a**/**3c**, 0.05 eV for **4c**/**4e**) challenges the limit of theoretical errors. Then, it is very hard to evaluate the accurate energies of large clusters of $Au^-(CH_3OH)_n$. Consequently, the main criterion of structural assignment should be the VDE instead of relative energy.

## 4. CONCLUSIONS

Gas-phase photoelectron spectroscopic and computational studies of methanol-solvated Au anionic clusters, $Au^-(CH_3OH)_n$ ($n$ = 0−5), have been performed. In the 266 nm photoelectron spectra, the bands of the ground and excited states of the solvated clusters are observed in the $Au^-(CH_3OH)_{1-2}$ clusters, while only the bands of the ground states are observed in the larger $Au^-(CH_3OH)_{3-5}$ clusters, due to the fact that the binding energies of the excited states are beyond the 266 nm photon energy. The comparison of theoretical results to the experimental data reveal that the nonconventional hydrogen bonds present in the range of $n$ = 1−5, while conventional hydrogen bonds become more and more important in the formation of solvated clusters at $n$ = 2−5. Such trend is supported by the calculated binding energies. Hence, the solvation process unveiled in photoelectron imaging provides possibility to get a microscopic insight into the transition dynamics at play in H-bond networks composed of a resticted number of methanol molecules around gold-anion chromophore.

## ■ ASSOCIATED CONTENT

### Supporting Information

Optimized structures at the mPW2PLYP/cc-pVDZ(pp) level and total binding energies ($E_b$, eV) of $Au^-(CH_3OH)_4$ at the mPW2PLYP/aug-cc-pVDZ(pp) level (Figure S1), theoretical VDEs of the low-lying isomers of $Au^-(CH_3OH)_4$ (Table S1), Cartesian coordinates of all structures at the mPW2PLYP/cc-pVDZ(pp) level (Table S2), and full author lists of refs 11 and 54. This material is available free of charge via the Internet at http://pubs.acs.org.

## ■ AUTHOR INFORMATION

### Corresponding Authors

*Telephone: +86-411-84379365. Fax: +86-411-84675584. E-mail: zctang@dicp.ac.cn (Z.T.).
*E-mail: ljiang@dicp.ac.cn (L.J.).
*E-mail: fanhj@dicp.ac.cn (H.J.F.).

### Notes

The authors declare no competing financial interest.

## ■ ACKNOWLEDGMENTS

This work is supported by the National Natural Science Foundation of China (Grant Nos. 21103186, 21073186, 21173212, and 21273233), the Ministry of Science and Technology of China (Grant Nos. 2011CB201301 and 2011YQ09000505), and the Chinese Academy of Sciences. L.J. acknowledges support from the Hundred Talents Program of Chinese Academy of Sciences.

## ■ REFERENCES

(1) Wild, D. A.; Bieske, E. J. Infrared Investigations of Negatively Charged Complexes and Clusters. *Int. Rev. Phys. Chem.* **2003**, *22*, 129−151.
(2) Duncan, M. A. Infrared Spectroscopy to Probe Structure and Dynamics in Metal Ion−Molecule Complexes. *Int. Rev. Phys. Chem.* **2003**, *22*, 407−435.
(3) Bieske, E. J. Spectroscopic Studies of Anion Complexes and Clusters: A Microscopic Approach to Understanding Anion Solvation. *Chem. Soc. Rev.* **2003**, *32*, 231.
(4) Ehrler, O. T.; Neumark, D. M. Dynamics of Electron Solvation in Molecular Clusters. *Acc. Chem. Res.* **2009**, *42*, 769−777.
(5) Wang, X. B.; Wang, L. S. Photoelectron Spectroscopy of Multiply Charged Anions. *Annu. Rev. Phys. Chem.* **2009**, *60*, 105−126.
(6) Wallace, W. T.; Wyrwas, R. B.; Whetten, R. L.; Mitrić, R.; Bonačić-Koutecký, V. Oxygen Adsorption on Hydrated Gold Cluster Anions: Experiment and Theory. *J. Am. Chem. Soc.* **2003**, *125*, 8408−8414.

(7) Bongiorno, A.; Landman, U. Water-Enhanced Catalysis of Co Oxidation on Free and Supported Gold Nanoclusters. *Phys. Rev. Lett.* **2005**, *95*, 106102.
(8) Kim, T. S.; Gong, J.; Ojifinni, R. A.; White, J. M.; Mullins, C. B. Water Activated by Atomic Oxygen on Au(111) to Oxidize Co at Low Temperatures. *J. Am. Chem. Soc.* **2006**, *128*, 6282−6283.
(9) Okumura, M.; Haruta, M.; Kitagawa, Y.; Yamaguchia, K. Theoretical Study of $H_2O$ and $O_2$ Adsorption on Au Small Clusters. *Gold Bull.* **2007**, *40*, 40−44.
(10) Ojifinni, R. A.; Froemming, N. S.; Gong, J.; Pan, M.; Kim, T. S.; White, J. M.; Henkelman, G.; Mullins, C. B. Water-Enhanced Low-Temperature CO Oxidation and Isotope Effects on Atomic Oxygen-Covered Au(111). *J. Am. Chem. Soc.* **2008**, *130*, 6801−6812.
(11) Lee, S.; Molina, L. M.; López, M. J.; Alonso, J. A.; Hammer, B.; Lee, B.; Seifert, S.; Winans, R. E.; Elam, J. W.; Pellin, M. J.; et al. Selective Propene Epoxidation on Immobilized $Au_{6-10}$ Clusters: The Effect of Hydrogen and Water on Activity and Selectivity. *Angew. Chem., Int. Ed.* **2009**, *48*, 1467−1471.
(12) Lyalin, A.; Taketsugu, T. Reactant-Promoted Oxygen Dissociation on Gold Clusters. *J. Phys. Chem. Lett.* **2010**, *1*, 1752−1757.
(13) Gao, Y.; Zeng, X. C. Water-Promoted $O_2$ Dissociation on Small-Sized Anionic Gold Clusters. *Acs. Catal.* **2012**, *2*, 2614−2621.
(14) Knurr, B. J.; Weber, J. M. Solvent-Driven Reductive Activation of Carbon Dioxide by Gold Anions. *J. Am. Chem. Soc.* **2012**, *134*, 18804−18808.
(15) Chang, C. R.; Yang, X. F.; Long, B.; Li, J. A Water-Promoted Mechanism of Alcohol Oxidation on a Au(111) Surface: Understanding the Catalytic Behavior of Bulk Gold. *ACS Catal.* **2013**, *3*, 1693−1699.
(16) Liu, C. Y.; Tan, Y. Z.; Lin, S. S.; Li, H.; Wu, X. J.; Li, L.; Pei, Y.; Zeng, X. C. CO Self-Promoting Oxidation on Nanosized Gold Clusters: Triangular $Au_3$ Active Site and CO Induced O−O Scission. *J. Am. Chem. Soc.* **2013**, *135*, 2583−2595.
(17) Shvartsburg, A. A.; Siu, K. W. M. Is There a Minimum Size for Aqueous Doubly Charged Metal Cations? *J. Am. Chem. Soc.* **2001**, *123*, 10071−10075.
(18) Duncombe, B. J.; Duale, K.; Buchanan-Smith, A.; Stace, A. J. The Solvation of $Cu^{2+}$ with Gas-Phase Clusters of Water and Ammonia. *J. Phys. Chem. A* **2007**, *111*, 5158−5165.
(19) Carl, D. R.; Moision, R. M.; Armentrout, P. B. Binding Energies for the Inner Hydration Shells of $Ca^{2+}$: An Experimental and Theoretical Investigation of $Ca^{2+}(H_2O)_x$ Complexes ($x$ = 5−9). *Int. J. Mass Spectrom.* **2007**, *265*, 308−325.
(20) Rodriguez-Cruz, S. E.; Williams, E. R. Gas-Phase Reactions of Hydrated Alkaline Earth Metal Ions, $M^{2+}(H_2O)_n$ (M = Mg, Ca, Sr, Ba and $n$ = 4−7), with Benzene. *J. Am. Soc. Mass. Spectrom.* **2001**, *12*, 250−257.
(21) Blades, A. T.; Jayaweera, P.; Ikonomou, M. G.; Kebarle, P. Studies of Alkaline Earth and Transition Metal $M^{+2}$ Gas Phase Ion Chemistry. *J. Chem. Phys.* **1990**, *92*, 5900.
(22) Peschke, M.; Blades, A. T.; Kebarle, P. Hydration Energies and Entropies for $Mg^{2+}$, $Ca^{2+}$, $Sr^{2+}$, and $Ba^{2+}$ from Gas-Phase Ion−Water Molecule Equilibria Determinations. *J. Phys. Chem. A* **1998**, *102*, 9978−9985.
(23) Leib, R. D.; Donald, W. A.; Bush, M. F.; O'Brie, J. T.; Williams, E. R. Internal Energy Deposition in Electron Capture Dissociation Measured Using Hydrated Divalent Metal Ions as Nanocalorimeters. *J. Am. Chem. Soc.* **2007**, *129*, 4894−4895.
(24) Leib, R. D.; Donald, W. A.; Bush, M. F.; O'Brien, J. T.; Williams, E. R. Nonergodicity in Electron Capture Dissociation Investigated Using Hydrated Ion Nanocalorimetry. *J. Am. Soc. Mass. Spectrom.* **2007**, *18*, 1217−1231.
(25) Wang, X. B.; Yang, X.; Wang, L. S. Probing Solution-Phase Species and Chemistry in the Gas Phase. *Int. Rev. Phys. Chem.* **2002**, *21*, 473−498.
(26) Stolow, A.; Bragg, A. E.; Neumark, D. M. Femtosecond Time-Resolved Photoelectron Spectroscopy. *Chem. Rev.* **2004**, *104*, 1719−1758.
(27) Young, R. M.; Neumark, D. M. Dynamics of Solvated Electrons in Clusters. *Chem. Rev.* **2012**, *112*, 5553−5577.
(28) Duncan, M. A. Spectroscopy of Metal Ion Complexes: Gas-Phase Models for Solvation. *Annu. Rev. Phys. Chem.* **1997**, *48*, 69−93.
(29) Lisy, J. M. Spectroscopy and Structure of Solvated Alkali-Metal Ions. *Int. Rev. Phys. Chem.* **1997**, *16*, 267−289.
(30) Ebata, T.; Fujii, A.; Mikami, N. Vibrational Spectroscopy of Small-Sized Hydrogen-Bonded Clusters and Their Ions. *Int. Rev. Phys. Chem.* **1998**, *17*, 331−361.
(31) Rathbone, G. J.; Sanford, T.; Andrews, D.; Lineberger, W. C. Photoelectron Imaging Spectroscopy of $Cu^-(H_2O)_{1,2}$ Anion Complexes. *Chem. Phys. Lett.* **2005**, *401*, 570−574.
(32) Schneider, H.; Boese, A. D.; Weber, J. M. Unusual Hydrogen Bonding Behavior in Binary Complexes of Coinage Metal Anions with Water. *J. Chem. Phys.* **2005**, *123*, 084307−6.
(33) Taylor, M. S.; Barbera, J.; Schulz, C.-P.; Muntean, F.; McCoy, A. B.; Lineberger, W. C. Femtosecond Dynamics of $Cu(H_2O)_2$. *J. Chem. Phys.* **2005**, *122*, 054310−11.
(34) Barbera, J.; Horvath, S.; Dribinski, V.; McCoy, A. B.; Lineberger, W. C. Femtosecond Dynamics of $Cu(CD_3OD)$. *J. Chem. Phys.* **2007**, *126*, 084307−10.
(35) Taylor, M. S.; Muntean, F.; Lineberger, W. C.; McCoy, A. B. A Theoretical and Computational Study of the Anion, Neutral, and Cation $Cu(H_2O)$ Complexes. *J. Chem. Phys.* **2004**, *121*, 5688−5699.
(36) Muntean, F.; Taylor, M. S.; McCoy, A. B.; Lineberger, W. C. Femtosecond Study of $Cu(H_2O)$ Dynamics. *J. Chem. Phys.* **2004**, *121*, 5676−5687.
(37) Zheng, W. J.; Li, X.; Eustis, S.; Grubisic, A.; Thomas, O.; de Clercq, H.; Bowen, K. Anion Photoelectron Spectroscopy of $Au^-(H_2O)_{1,2}$, $(D_2O)_{1-4}$, and $AuOH^-$. *Chem. Phys. Lett.* **2007**, *444*, 232−236.
(38) Gao, Y.; Huang, W.; Woodford, J.; Wang, L. S.; Zeng, X. C. Detecting Weak Interactions between Au− and Gas Molecules: A Photoelectron Spectroscopic and Ab Initio Study. *J. Am. Chem. Soc.* **2009**, *131*, 9484−9485.
(39) Chi, C. X.; Xie, H.; Li, Y. Z.; Cong, R.; Zhou, M. F.; Tang, Z. C. Photoelectron Imaging of $Ag^-(H_2O)_x$ and $AgOH^-(H_2O)_y$ (x = 1,2, y = 0−4). *J. Phys. Chem. A* **2011**, *115*, 5380−5386.
(40) Chi, C. X.; Xie, H.; Cong, R.; Tang, Z. C.; Zhou, M. F. Photoelectron Imaging of $AgOCH_3^-$ and $Ag^-(CH_3OH)_x$ (x = 1, 2). *Chin. J. Chem. Phys.* **2011**, *24*, 557−562.
(41) Li, X.; Ko, Y. J.; Wang, H.; Bowen, K. H.; Guevara-Garcia, A.; Martinez, A. Photoelectron and Computational Studies of the Copper-Nucleoside Anionic Complexes, $Cu^-$(Cytidine) and $Cu^-$(Uridine). *J. Chem. Phys.* **2011**, *134*, 054318.
(42) Cao, G. J.; Xu, H. G.; Li, R. Z.; Zheng, W. Hydrogen Bonds in the Nucleobase-Gold Complexes: Photoelectron Spectroscopy and Density Functional Calculations. *J. Chem. Phys.* **2012**, *136*, 014305.
(43) Tachikawa, H. Electron Detachment Dynamics of $Cu^-(H_2O)_n$ ($n$ = 1−3): A Direct Ab Initio Md Study. *RSC Adv.* **2012**, *2*, 12346−12354.
(44) Qin, Z. B.; Cong, R.; Wu, X.; Liu, Z. L.; Xie, H.; Tang, Z. C.; Jiang, L.; Fan, H. J. Photoelectron Velocity-Map Imaging Spectroscopic and Theoretical Study on the Reactivity of the Gold Atom toward $CH_3SH$, $CH_3OH$, and $H_2O$. *J. Chem. Phys.* **2013**, *139*, 034315.
(45) Walker, N. R.; Walters, R. S.; Duncan, M. A. Frontiers in the Infrared Spectroscopy of Gas Phase Metal Ion Complexes. *New J. Chem.* **2005**, *29*, 1495−1503.
(46) Iino, T.; Ohashi, K.; Inoue, K.; Judai, K.; Nishi, N.; Sekiya, H. Infrared Spectroscopy of $Cu^+(H_2O)_n$ and $Ag^+(H_2O)_n$: Coordination and Solvation of Noble-Metal Ions. *J. Chem. Phys.* **2007**, *126*, 194302.
(47) Iino, T.; Ohashi, K.; Inoue, K.; Judai, K.; Nishi, N.; Sekiya, H. Coordination and Solvation of Noble Metal Ions: Infrared Spectroscopy of $Ag^+(H_2O)_n$. *Eur. Phys. J. D* **2007**, *43*, 37−40.
(48) Iino, T.; Ohashi, K.; Mune, Y.; Inokuchi, Y.; Judai, K.; Nishi, N.; Sekiya, H. Infrared Photodissociation Spectra and Solvation Structures of $Cu^+(H_2O)_n$ ($n$ = 1−4). *Chem. Phys. Lett.* **2006**, *427*, 24−28.
(49) Miller, D. J.; Lisy, J. M. Hydrated Alkali-Metal Cations: Infrared Spectroscopy and Ab Initio Calculations of $M^+(H_2O)_{x=2-5}Ar$ Cluster

Ions for M = Li, Na, K, and Cs. *J. Am. Chem. Soc.* **2008**, *130*, 15381−15392.
(50) Miller, D. J.; Lisy, J. M. Entropic Effects on Hydrated Alkali-Metal Cations: Infrared Spectroscopy and Ab Initio Calculations of $M^+(H_2O)_{x=2-5}$ Cluster Ions for M = Li, Na, K, and Cs. *J. Am. Chem. Soc.* **2008**, *130*, 15393−15404.
(51) Cabarcos, O. M.; Weinheimer, C. J.; Martínez, T. J.; Lisy, J. M. The Solvation of Chloride by Methanol-Surface Versus Interior Cluster Ion States. *J. Chem. Phys.* **1999**, *110*, 9516.
(52) Vargas, R.; Garza, J.; Dixon, D. A.; Hay, B. P. How Strong Is the $C^{\alpha}$−H···O=C Hydrogen Bond? *J. Am. Chem. Soc.* **2000**, *122*, 4750−4755.
(53) Ramírez, J.-Z.; Vargas, R.; Garza, J. The Role of the Linearity on the Hydrogen Bond in the Formamide Dimer: A BLYP, B3LYP, and MP2 Study. *J. Mex. Chem. Soc.* **2008**, *52*, 31−35.
(54) Valdespino-Saenz, J.; Martínez, A. Theoretical Study of Neutral, Anionic, and Cationic Uracil−Ag and Uracil−Au Systems: Non-conventional Hydrogen Bonds. *J. Phys. Chem. A* **2008**, *112*, 2408−2414.
(55) Vargas, R.; Martínez, A. Non-Conventional Hydrogen Bonds: Pterins-Metal Anions. *Phys. Chem. Chem. Phys.* **2011**, *13*, 12775−12784.
(56) Qin, Z. B.; Wu, X.; Tang, Z. C. Note: A Novel Dual-Channel Time-of-Flight Mass Spectrometer for Photoelectron Imaging Spectroscopy. *Rev. Sci. Instrum.* **2013**, *84*, 066108.
(57) Dribinski, V.; Ossadtchi, A.; Mandelshtam, V. A.; Reisler, H. Reconstruction of Abel-Transformable Images: The Gaussian Basis-Set Expansion Abel Transform Method. *Rev. Sci. Instrum.* **2002**, *73*, 2634−2642.
(58) Frisch;, M. J.; Trucks;, G. W.; Schlegel;, H. B.; Scuseria;, G. E.; Robb;, M. A.; Cheeseman;, J. R.; Scalmani, G.; Barone;, V.; Mennucci;, B.; Petersson;, G. A.; et al. Gaussian 09, Revision A02, Gaussian, Inc.: Wallingford, CT, 2009.
(59) Schwabe, T.; Grimme, S. Towards Chemical Accuracy for the Thermodynamics of Large Molecules: New Hybrid Density Functionals Including Non-Local Correlation Effects. *Phys. Chem. Chem. Phys.* **2006**, *8*, 4398−4401.
(60) Peterson, K. A.; Puzzarini, C. Systematically Convergent Basis Sets for Transition Metals. Ii. Pseudopotential-Based Correlation Consistent Basis Sets for the Group 11 (Cu, Ag, Au) and 12 (Zn, Cd, Hg) Elements. *Theor. Chem. Acc.* **2005**, *114*, 283−296.
(61) Dunning, J. T. H. Gaussian Basis Sets for Use in Correlated Molecular Calculations. I. The Atoms Boron through Neon and Hydrogen. *J. Chem. Phys.* **1989**, *90*, 1007−1023.
(62) Kendall, R. A.; Dunning, J. T. H.; Harrison, R. J. Electron Affinities of the First-Row Atoms Revisited. Systematic Basis Sets and Wave Functions. *J. Chem. Phys.* **1992**, *96*, 6796−6806.
(63) Woon, D. E.; Dunning, J. T. H. Gaussian Basis Sets for Use in Correlated Molecular Calculations. III. The Atoms Aluminum through Argon. *J. Chem. Phys.* **1993**, *98*, 1358−1371.
(64) Boys, S. F.; Bernardi, F. The Calculation of Small Molecular Interactions by the Differences of Separate Total Energies. Some Procedures with Reduced Errors. *Mol. Phys.* **1970**, *19*, 553−566.
(65) Simon, S. l.; Duran, M.; Dannenberg, J. J. How Does Basis Set Superposition Error Change the Potential Surfaces for Hydrogen-Bonded Dimers? *J. Chem. Phys.* **1996**, *105*, 11024.
(66) Wu, X.; Tan, K.; Tang, Z. C.; Lu, X. Hydrogen Bonding in Microsolvation: Photoelectron Imaging and Theoretical Studies on $Au_x^-(H_2O)_n$ and $Au_x^-(CH_3OH)_n$ ($x$ = 1, 2; $n$ = 1, 2) Complexes. *Phys. Chem. Chem. Phys.* **2014**, *16*, 4771.
(67) Etter, M. C. Encoding and Decoding Hydrogen-Bond Patterns of Organic Compounds. *Acc. Chem. Res.* **1990**, *23*, 120−126.
(68) Grabowski, S. J. Ab Initio Calculations on Conventional and Unconventional Hydrogen Bonds-Study of the Hydrogen Bond Strength. *J. Phys. Chem. A* **2001**, *105*, 10739−10746.
(69) Reed, A. E.; Curtiss, L. A.; Weinhold, F. Intermolecular Interactions from a Natural Bond Orbital, Donor-Acceptor Viewpoint. *Chem. Rev.* **1988**, *88*, 899−926.